International Journal of Engineering Research and Technology.
ISSN 0974-3154 Volume 11, Number 12 (2018), pp. 1837-1850
© International Research Publication House
http://www.irphouse.com

Computer simulation of the submerged arc welding process on the basis of self-consistent physico-mathematical model

S.S. Miller

Welding Department, Tula State University, Tula, Russia

ABSTRACT

Computer simulation of the submerged arc welding process is based on solving a self-consistent physico-mathematical model. This means that the developed simulation is based on the some of the most complete physical-mathematical model of the submerged-arc welding process. This model includes submodels of the heat sources, heat transfer, electromagnetic phenomena in the weld pool, hydrodynamic phenomena in the weld pool, and submodel of free surfaces of the weld pool. This physico-mathematical model is the basis of the developed software for the simulation of the submerged-arc welding process (SAW).

Keywords: Computer engineering, numerical model, simulation, welding.

I. INTRODUCTION

When creating new products and innovative technologies, we have to perform time-consuming experimental research, the task of which is to optimize the technological process. The need for research usually arises when creating new objects, using new materials and equipment.

To reduce the cost of such research and to optimize the manufacturing technology of the object, it is advisable to use a preliminary theoretical study based on computer simulation of the phenomena in the object of study, i.e. computer-aided engineering.

In the modern world, computer-aided engineering (CAE) systems are widely used, allowing simulate various physical processes occurring in the objects of study.

There are known theoretical models of arc welding [1-8], which are based on the system of heat transfer equations and equilibrium of the weld pool surface. These models reproduce well the formation of the weld pool and weld in shielded gas welding. However, these models were not able to reproduce the formation of a seam during arc welding under a layer of flux.

In particular, the known models of arc welding do not reproduce the formation of specific seam formation under a flux layer, which is characterized by the mushroom-

shaped cross section of the seam (Fig. 1) as well as the strong dependence of this form on the arc voltage and the electrode diameter (Fig. 2).

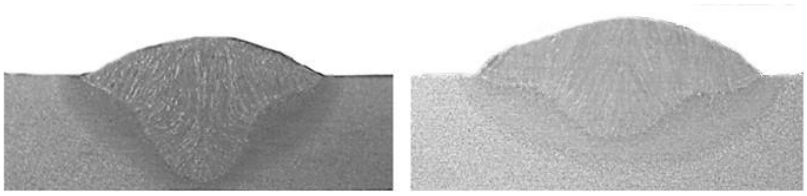

a) b)

Fig.1. Profiles of weld penetrations in carbon dioxide (a) and under a layer of flux (b) in the same welding conditions

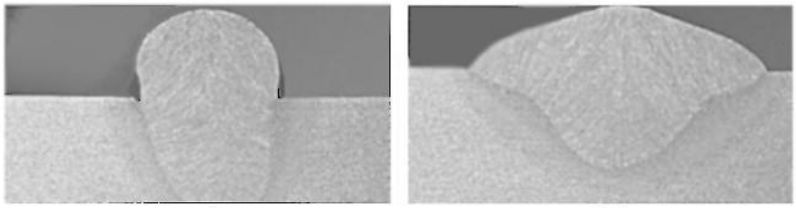

a) b)

Fig.2. The effect of voltage 25V (a) and 35V (b) on the cross-profile of the weld during welding under flux at the same arc current and welding speed.

II. PHENOMENOLOGICAL ANALYSIS

Obviously, the main difference between submerged-arc welding and gas-shielded arc welding is that the arc is in the gas cavity formed by flux vapors. As the arc moves, the flux in front of the arc melts and partially evaporates, and behind the arc it condenses and hardens. These phenomena significantly change the heat transfer in the formation zone of the weld pool and can explain the difference in the seam profiles.

The effect of arc voltage on the seam profile can be explained by the fact that as the arc voltage increases, the length and power of the plasma arc column also increases, hence the volume of the flux vapor in the arc cavity increases. Increasing the arc length increases the cavity height and redistributes the energy of the flux vapor to the metal surface, which increases the seam width on the surface of the weldment. At low voltage and short arc, the gas cavity is located deep in the metal, respectively, narrow seams are formed.

A noticeable effect of the electrode diameter on the formation of a weld in submerged-arc welding is associated with the use of large-diameter wires. Since, with an equal arc current, the same amount of electrode metal is melted, as the wire diameter increases, the electrode feed rate should be reduced to obtain a given arc current. Accordingly, the pressure of the droplets of the electrode metal on the surface of the weld pool will decrease, which will reduce the deflection of the surface of the weld pool and reduce the depth of penetration.

III. MATHEMATICAL MODEL

To explain the above features of submerged-arc welding, submodels of these phenomena were introduced into the well-known model of weld formation.

III.I. SIMULATION SPACE AND COORDINATE SYSTEM

In the simulation process was used fixed Cartesian coordinate system x, y, *z* (Fig. 3), in which the metal of the welded joint is immobile, and the electrode and the arc move with a welding speed v_w in the direction of the x coordinate.

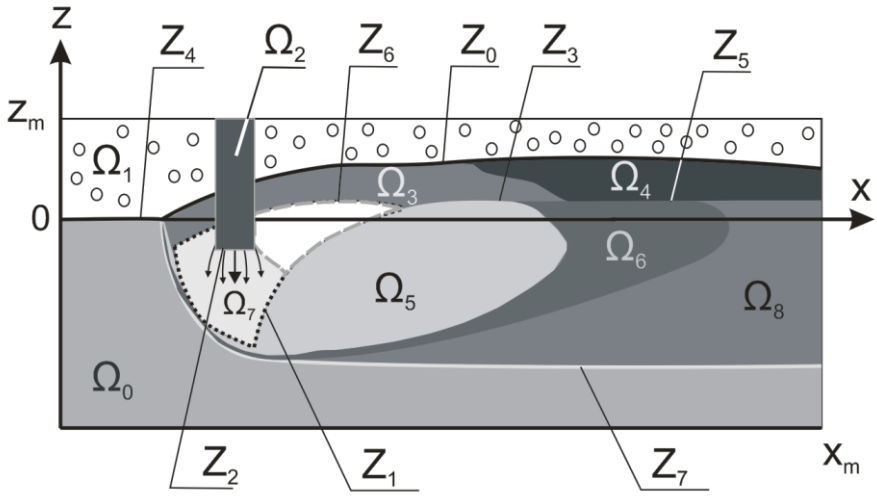

Fig.3. The structure of the simulation zone: Ω0 – base metal, Ω1 – powder flux, Ω2 – electrode, Ω3 –molten slag, Ω4 –solid slag, Ω5 – molten metal, Ω6 – solid-liquid metal, Ω7 – flux vapor and Ω8 – weld metal.

Internal interphase boundaries are defined as intersections of sets Ω and denoted by:

- Z0=Ω1∩Ω3 (powder flux - slag), is determined by the decomposition of the solidification flux isotherm;
- Z1=Ω7∩Ω5) (flux vapor - molten metal), is determined by the solution of the equilibrium equation of the surface of the weld pool;
- Z2=Ω7∩Ω2 (electrode - arc), defined as the distance from the surface of the weld pool, equal to the length of the arc;
- Z3=Ω3∩Ω5 (molten metal - molten slag), is determined by solving the equilibrium equation of the surface of the weld pool;
- Z4=Ω0∩Ω1 (solid metal - powder flux), determined by the profile of the groove;
- Z5=Ω4∩(Ω6∪Ω8) (solid slag - metal), is determined by the location of the surface of the weld pool on the crystallization line;
- Z6= Ω7∩Ω3 (flux vapor - slag), is determined by the location of the isotherm of evaporation of the flux;
- Z7= Ω0∩Ω8 (base metal - seam), is determined by the limiting distribution of the melting point of the metal.

III.II. DIFFERENTIAL HEAT EQUATION

The main equation in the simulation is a nonstationary nonlinear heat equation with boundary conditions, which determines the enthalpy change rate at different points of the weld metal (1).

$$\frac{\partial H}{\partial t} = \frac{\partial}{\partial x}\left(\lambda \frac{\partial T}{\partial x}\right) + \frac{\partial}{\partial y}\left(\lambda \frac{\partial T}{\partial y}\right) + \frac{\partial}{\partial z}\left(\lambda \frac{\partial T}{\partial z}\right) + v_x \frac{\partial H}{\partial x} + q, \tag{1}$$

where $H = H(x,y,z,t)$ – is a bulk enthalpy, J/cm^3; $\lambda=\lambda(x,y,z,t)$ – coefficient of thermal conductivity, W/cm·grad, v_x – movement speed of liquid metal, $q=q(x,y,z)$ – heat intensity distribution of the welding arc , W/cm^3.

The enthalpy $H=H(x,y,z,t)$ is related to the temperature T by a non-linear function that takes into account the fusion heat H_{LS} and the heat capacity $c\rho$ of the substance located at a given point in the simulation space (Fig. 3) .

Boundary conditions:

At the boundaries of the simulation area x=0, y=0, z=0, x=xm, y=ym, z=zm, linear interpolation $T(x,y,z,t)$ of the equation to the boundaries is used:

$$\frac{\partial^2 T}{\partial n^2} = 0 \tag{2}$$

where n – is the normal to the boundary surface.

Initial conditions:

$$t = 0,\ T(x, y, z) = T0, \tag{3}$$

correspond to the beginning of the welding process, i.e. it is assumed that at the initial moment the temperature of the fusion faces in all points is equal to the ambient temperature. The structure of the modeling space (Fig. 3), was taken in accordance with the moment of arc initiation: the location of the metal corresponds to the geometry of groove, the flux is in a powder state, the electrode contacts the metal surface, the welding pool and the gas cavity are absent.

III.III. HEAT INTENSITY DISTRIBUTION OF THE WELDING ARC

$q=q(x_a,y,z)$ in the modeling space is determined according to physical phenomena in the arc cavity and adjacent zones, as well as with the movement of the arc axis $x_a=x_0+v_w t$ in the modeling zone with the welding speed v_w.

The heating of electrode stick-out by arc current (zone Ω2):

$$\frac{dT_f}{dz} = \frac{\rho_e j^2}{c\rho_f} \frac{y_m - y}{v_f}, \tag{4}$$

where T_f – temperature of electrode stick-out, $\rho_e = \rho_e(T_f)$ – volume resistivity, $j = \frac{4I}{\pi d_f^2}$ - current density I in an electrode with a diameter d_f, $c\rho_f$ – volumetric heat capacity of the electrode material, v_f – electrode feed.
The anode area of the arc (surface Z2=Ω7∩Ω2):

$$\frac{dq}{dz} = jU_a, \tag{5}$$

where U_a – voltage drop in the anode region of the arc.

The heat liberation in the plasma flame of the arc is described as the distribution of radiation of the arc column over the surface of the arc cavity Ω7 (surface Z1=Ω7∩(Ω3∪Ω5)):

$$\frac{dq}{dn} = \frac{EIL}{r^2}, \tag{6}$$

where E – potential gradient in arc column, I,L – arc current and arc length, r – the distance between the point of the surface Z1 and the center of the arc column.

The cathode region of the arc (surface Z1=Ω7∩Ω5):

$$\frac{dq}{dn} = \frac{IU_k}{\pi R^2}\exp\left(-\frac{r_0^2}{R^2}\right), \tag{7}$$

where U_k – cathode arc voltage, R – effective arc radius, r_0 – the distance between the point of the surface Z1 and the point of intersection of the arc axis with the surface Z1.

Heat transfer by droplets of an electrode metal is described as heat release on the surface (surface Z1=Ω7∩Ω5):

$$\frac{dq}{dn} = \frac{4c\rho T_k v_f}{\pi d_f^2}\exp\left(-\frac{4r_0^2}{d_f^2}\right), \tag{8}$$

where T_k – temperature of droplets.

Heat liberation in the liquid slag is practically absent, so the slag does not have direct contact with the electrode, which has a temperature below the melting point of the flux, and the electrical resistance of the powder flux is very high.

IV. EQUILIBRIUM EQUATION OF THE WELD POOL SURFACE

The location of the surface of the weld pool $Z(x,y)=\Omega 5\cap(\Omega 7\cup\Omega 3)$ is determined by the pressure equilibrium equation (9): capillary pressure p_σ, gravitational pressure p_g, the flow of the electrode metal droplets p_f, hydrodynamic pressure of metal flow in a weld pool p_v, electrodynamic pressure arc p_a, internal pressure of liquid metal p_m.

$$p_\sigma + p_a + p_f + p_v + p_g + p_m = 0, \tag{9}$$

Capillary pressure is determined by the curvature of the surface $Z(x,y)$ and for small deflections it is determined as:

$$p_\sigma = -\sigma\left(\frac{\partial^2 Z}{\partial x^2} + \frac{\partial^2 Z}{\partial y^2}\right), \tag{10}$$

where σ - surface tension coefficient.

Gravitational pressure is determined by the weight of a column of substance above the surface point of the weld pool:

$$p_g = g\left(\rho\left(Z - z_{\max}\right) + \rho_h Z_h\right), \tag{11}$$

where - g – acceleration of gravity, ρ, ρ_h – metal and slag densities, z_{max} – maximum surface height of the weld pool, Z_h – thickness of the liquid slag layer.

Electrodynamic pressure of the arc is determined by the arc current:

$$p_a = \frac{k_a I^2}{\pi R_p^2}\exp\left[-\frac{\left(x_0 + v_w t\right)^2 + y^2}{R_p^2}\right], \tag{12}$$

where - k_a - electrodynamic coefficient, R_p- arc force radius.

The flow pressure of the droplets of the electrode metal is determined by the speed and mass of the flow:

$$p_f = \rho\frac{v_f^2}{2}\exp\left[-\frac{\left(x_0 + v_w t\right)^2 + y^2}{R_f^2}\right], \tag{13}$$

The velocity of liquid metal v_x in the weld pool $\Omega 5$ is determined by the ratio between the flow of liquid metal and the cross section of the weld pool:

$$v_x(x) = v_w\frac{Z1(x,y) - Z5(x,y)}{Z1(x,y) - Z7(x,y)}, \tag{14}$$

where - v_w – welding speed.

The hydrodynamic pressure of the weld pool metal flow is determined by the change rate of the weld pool cross-section area (15).

$$p_v = -\rho v_x^2\frac{dS_{\Omega 5}}{dx}, \tag{15}$$

This pressure component increases the pressure before the arc and decreases it behind the arc.

The internal pressure in the melt p_m is determined from the equality of equality of the area of the weld metal to the amount of electrode metal consumed in solving the variation problem:

$$S_{\Omega 8+\Omega 0}(x_m) - S_{\Omega 0}(0) \xrightarrow{p_m = \mathrm{var}} \pi r_f \frac{v_f}{v_w}, \tag{16}$$

where - $S_{\Omega 8+\Omega 0}(x_m)$ – the cross-sectional area of the seam at the end of the modeling area $x=x_m$, $S_{\Omega 0}(0)$ - the initial cross-sectional area of the groove edges at x=0.

V. CURRENT AND WELDING ARC LOCATION

The arc current I is set by the feed rate v_f and the diameter d_f of the electrode:'

$$I = v_f \frac{\pi d_f^2}{4}\left(c\rho_f\left(T_k - T_f\right) + H_{LS}\right), \tag{17}$$

where - T_k – is the temperature of the electrode droplets, H_{LS} – is the volume heat of fusion.

The length L of the welding arc is given by the voltage U_0 of the power source and depends on the electrical resistance of the current-carrying elements R_0 and electrode stick-out R_f:

$$L = \frac{1}{E}\left(U_0 - U_a - U_k - I\left(R_0 + R_f\right)\right), \tag{18}$$

The electrode stick-out resistance depends on its length L_f and the temperature T_f, distributed over the length:

$$R_f = \frac{4}{\pi d_f^2}\int_0^{L_f} \rho_e\left(T_f(z)dz\right), \tag{19}$$

VI. CORRECTION OF THE SIMULATION AREA STRUCTURE

The initial uncertainty of the weld pool geometric structure formation requires a continuous change in the location of the interfacial surfaces depending on the results of solving the equilibrium equation of the weld pool.

When transferring the surface $Z(x,y)=\Omega 5\cap(\Omega 7\cup\Omega 3)$ it is assumed that the temperature of the metal and slag in the zone of displacement is equal to the surface temperature, and their enthalpies change in accordance with this temperature. The resulting error is defined as the rate of change of enthalpy during surface transfiguration:

$$\Lambda_{\Omega 3} = \frac{d}{dt}\left(\int_{\Omega 3} H d\Omega\right),$$
$$\Lambda_{\Omega 5} = \frac{d}{dt}\left(\int_{\Omega 5} H d\Omega\right) \tag{20}$$

These errors are compensated by changing the enthalpy of the zones Ω3 and Ω5 depending on the temperature distribution:

$$\Delta H\left((x,y,z)\in\Omega 3\right) = \Lambda \frac{T(x,y,z)-T_L}{\frac{1}{\Omega_3}\int_{\Omega 3}\left(T(x,y,z)-T_L\right)d\Omega}, \tag{21}$$

where - T_L – liquidus temperature.

As the thermodynamic state approaches the steady state, the transformation error is defined as $\Lambda_\Omega \to 0$.
The condition for the end of the simulation is the stabilization of the solidus isotherm length:

$$\frac{d}{dt}\left(x_{\max} \in \Omega 6\right) \to 0, \tag{22}$$

Solving the model equation systems in the form of temperature distributions *T(x,y,z,t)* and the geometric structure of the modeling zone *Ω(t)* allows the initial stage of the process to be reproduced from the moment of arc initiation until the steady-state weld pool.

VII. NUMERICAL SOLUTION OF THE SELF-CONSISTENT PHYSICO-MATHEMATICAL MODEL

A feature of the submerged arc welding model is the complexity of the weld pool formation zone, for the numerical description of which a discrete space is used, which consists of a set of points evenly spaced with a step *Δ*. The continuous coordinates *x,y,z* of points are replaced by indices *i,j,k*. The structure of a discrete space is defined by an array of pointers $\Omega_{i,j,k}$ belonging to a point *i,j,k* to a flux in a powder, liquid, vaporous and melted state, or to a metal in a solid or liquid state. Depending on the current result of solving the system of equations of the model, the structure of the array $\Omega_{i,j,k}$ varies.
To solve the equations of heat conduction and equilibrium of the weld pool surface, the finite difference method on conjugate grids was used. On the interfacial surfaces, the coefficient of thermal conductivity was determined as the average harmonic value of thermal conductivities of adjacent phases.

To reduce the size of the modeling zone as the electrode moves to the grid step, i.e. in time $\tau=\Delta/v_w$, the array of pointers is translated, on one node against the direction of welding:

$$\Omega_{i,j,k}(t)=\Omega_{i+1,j,k}(t-\tau),$$
$$H_{i,j,k}(t)=H_{i+1,j,k}(t-\tau), \qquad (23)$$
$$T_{i,j,k}(t)=T_{i+1,j,k}(t-\tau),$$

In this case, the coordinate of the arc axis returns to its original position $x_a=x_0$.
Figure 4 presents the algorithm for numerical simulation of the submerged-arc welding process.

Initial data: geometry of groove after the previous pass, the thermophysical properties of steel and flux, welding parameters **Determination of the initial geometry of the numerical solution zone** **Calculation of electrode melting parameters and energy characteristics of the welding arc**
The cycle of non-stationary numerical simulation of the thermodynamic state of the formation of the weld pool
Determination of distribution of heat fluxes on metal and slag surfaces **Solution of heat equation**
The solution of the variation problem of the location of the welding arc in the groove
The solution of the equilibrium equation of the surface of the weld pool when exposed to capillary, gravitational, electrodynamic, hydrodynamic and internal pressures
Calculation of the internal pressure of the weld pool according to the condition of mass balance of the weld and electrode feed
until equal masses of surfacing and electrode feed
Correction of the location of the interphase boundaries "vapor-slag-powder, flux-solid slag", "solid-liquid metal" by solving the equation of heat conduction and equilibrium of the weld pool surface
until the stabilization the length of the solidus isotherm
Formation of simulation results documents: temperature distribution, geometry of the weld pool formation area, energy characteristics of the welding process

Fig.4. Algorithm for numerical simulation of weld formation in submerged arc welding

VIII. SIMULATION RESULTS:

Figure 5 shows the result of computer simulation of the welding process under the “AN-348A” flux with a grain fraction of 0.5-1.0 mm of a double-groove preparation joint “S25” of 20 mm in thickness, from “09G2C” steel with the “Sv08G2S” electrode wire.

Process parameters: arc power supply voltage 30 V, electric resistance of the welding circuit with electrode stick-out is 4 mΩ, welding speed is 5 mm / s, electrode diameter 4.0 mm, electrode feed rate 24 mm / s, stick-out is 30 mm.

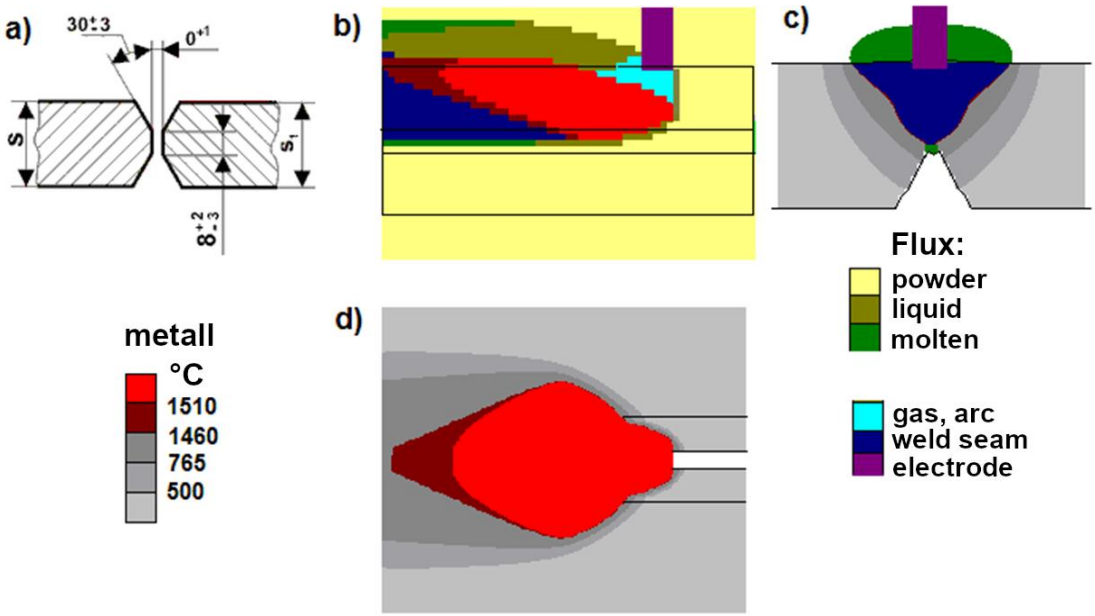

Fig.5. The simulation result of the weld formation process for a welding double-groove preparation joint from steel "09G2S" 20 mm: a) cross-sectional drawing of a groove b) longitudinal section of the modeling zone, c) calculated cross-section profile of the seam d) top view of the metal surface

The results obtained during the simulation process: arc current is 650 A, arc length is 2.6 mm, effective anode voltage drop - 5.8 V, cathode voltage drop - 9.5 V, potential gradient in the arc column 5.3 V / mm, arc diameter 17 mm, heating the electrode to a temperature 220 °C, stick-out resistance - 0.7 mΩ. The total power of the process is 19 kW, from which the radiation is 8.8 kW; the arc emits 4.1 kW at the electrode, and 6.1 kW at the joint surface. The heat liberation power of the electrode stick-out is 0.3 kW, the temperature of its heating by the arc current is 235°C. The length of the weld pool is 30 mm for the liquidus temperature, 40 mm for the solidus temperature, the maximum width is 23 mm, and the depth is 11 mm. The cross-sectional area of the seam is 140 mm^2, the weld metal 50 mm^2, the heat-affected zone is 86 mm^2, the remolten flux area - 94 mm^2.

The effect of the voltage of the power source and the diameter of the electrode wire was simulated when the plate of "09G2S" 12 mm in thickness was welded at a welding speed of 5 mm/s, and an arc current was 480 A. The electrode feed rate was adjusted to obtain the specified current value.

The simulation results for different values of the arc voltage (24V and 40V) and for the electrode diameter 3 mm are shown in Figure 6. Modeling showed that at a voltage of 24V, the length and voltage of the arc column are 1.8 mm and 8 V,

respectively. With an increase in the source voltage to 40 V, the length and voltage of the column increase to 5.4 mm and 24 V, respectively. At the same time, the weld pool depth has not changed much, but the melting end of the electrode at high voltage is higher. The increase in the power of the arc column and the area of its contact with the flux markedly changed the amount of evaporated and remelted flux. Since most of the heat spent on evaporation and melting of the flux is transferred to the surface of the weld pool due to the low thermal conductivity of the powder flux covering the welding zone, this leads to a very noticeable change in the shape of the weld. This increase in voltage led to an increase in the width of the seam from 9 to 16.4 mm and a decrease in its convexity from 4 mm to 2.2 mm, while the bath length increased from 18 to 25 mm. The average thickness of the layer of remelted flux increased from 0.9 to 2 mm.

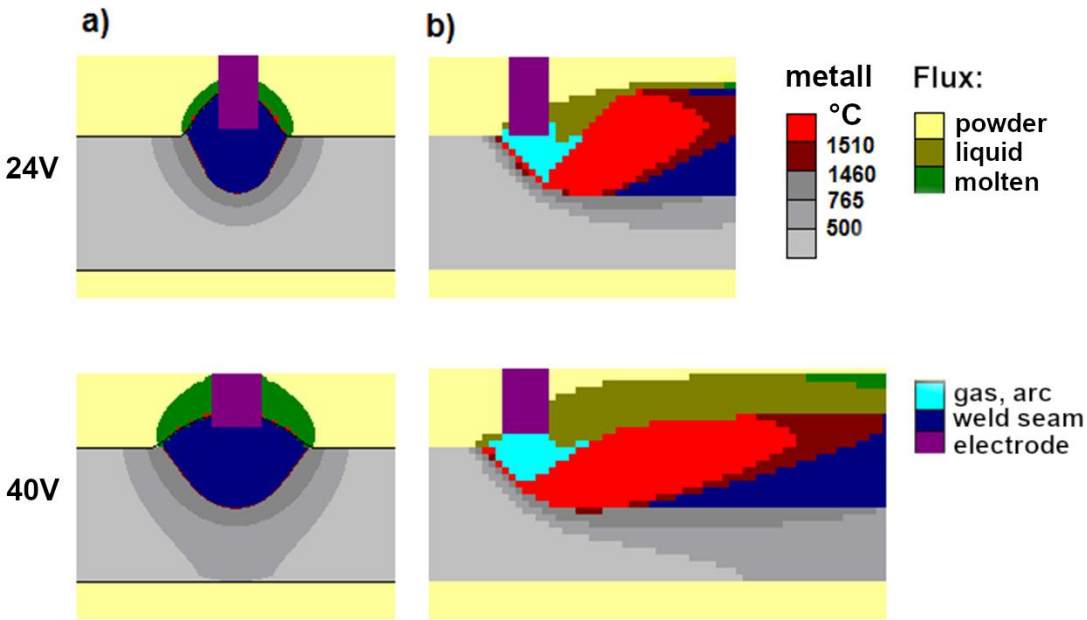

Fig.6. The results of the penetration simulation of a plate made of steel 09G2S - 12 mm in thickness under a layer of flux, at different values of the arc power source voltage (24V and 40V): a) limiting temperature distribution in the weld cross section, b) temperature and flux distribution in the longitudinal plane of symmetry

The simulation results for different values of the diameter of the electrode wire (2 and 4 mm) and the voltage of the power source of the 32 V arc are shown in Figure 7. The simulation showed that to maintain the same welding current (480 A), it is necessary to change the feed rate strongly: with a 2 mm electrode diameter, the feed rate is 79 mm/s, and at 4 mm - 15 mm/s. This change is more significant than the change in the ratio of the electrode cross section area, since the temperature of heating of the electrode stick-out by the current passing through it (830°C at 2 mm and 140°C at 4 mm) varies greatly. Therefore, the amount of heat transferred by droplets of the electrode metal to the weld pool with the electrode diameter increases slightly (in this case, 1.4 times), but the area of droplets expansion increases (by 4 times).

Therefore, the concentration of heat input drops under the electrode increases very significantly, which has a significant impact on the penetration depth. In this case, with an electrode diameter of 2 mm, the penetration depth was 8.1 mm, and at 4 mm - 5.6 mm. The pressure of the droplet flow, determined by the feed rate of the electrode, varies very significantly. Therefore, the depth of the crater under the arc with a small diameter electrode is much greater. Since the voltage and the length of the arc weakly depend on the diameter of the electrode, the arc column with a small diameter buried in the weld pool, respectively, the power of heat generation in the column is spent mainly on the melting of the metal, and not the flux. Accordingly, the thickness of the remelted flux above the seam with a small diameter of the electrode is somewhat less than with a large (1 and 3 mm, respectively). The width of the seam and the length of the bath is also slightly smaller, since the diameter of the electrode at a given arc current almost does not affect the power released in the arc column.

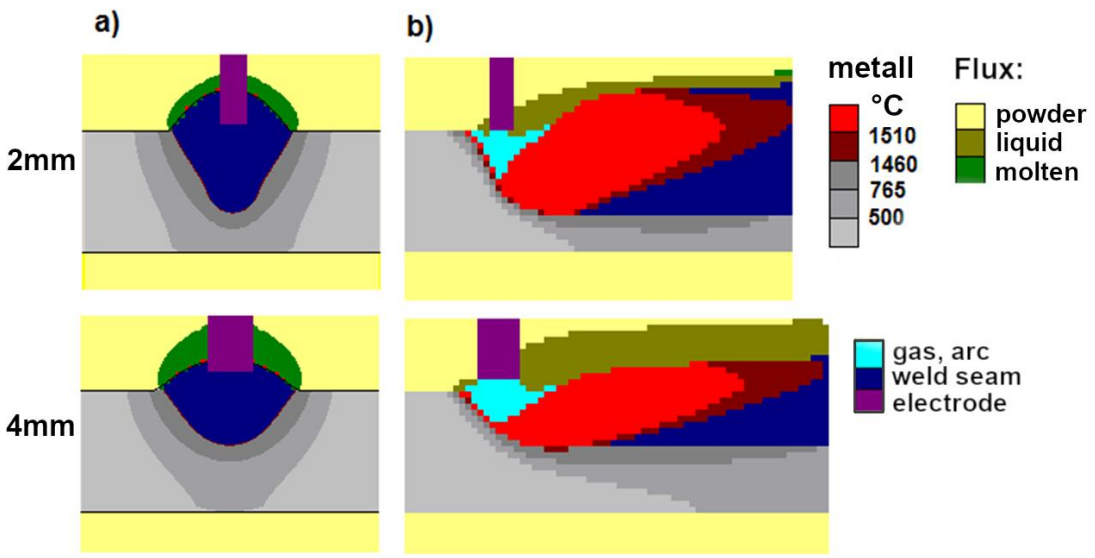

Fig.7. The results of the penetration simulation of a plate from steel 09G2S 12 mm in thickness under a layer of flux, for different values of the electrode diameter (2 and 4 mm): a) limit temperature distribution in the cross section of the weld, b) temperature and flux distribution in the longitudinal plane of symmetry

IX. COMPARISON WITH EXPERIMENTAL DATA

The obtained simulation results explain the results of experiments (Fig.1). The difference in the results of welding in carbon dioxide and under a flux layer with the same arc current is due to the fact that when welding in shielding gases, the power of the arc column is almost completely radiated into the open space, and under the flux beam much of this power is transmitted by steam and melt flux from the weld pool surface. This changes the cross-sectional profile of the seam - when welding under flux, the seams have a characteristic extension at the top. The strong influence of the power supply voltage on the penetration profile during submerged-arc welding is explained by the change in the power of the arc column, which is spent mainly on the

evaporation of the flux and subsequent condensation on the surface of the weld pool, respectively, the weld width greatly increases. The depth of penetration is determined mainly by the electrodynamic pressure of the arc, which is determined by the specified arc current. The influence of the electrode wire diameter on the depth of penetration is associated with a change in the concentration of the heat flux and the electrode drop pressure on the surface of the weld pool and the depth of the crater under the arc.

CONCLUSIONS

Based on the comparison of simulation results and experimental data, it was established that:

- A self-consistent physico-mathematical model of the submerged-arc welding process was developed based on the system of heat and mass transfer equations, hydrodynamic phenomena in the weld pool, and pressure equilibrium on the weld pool surface, taking into account heat transfer in the arc column with flux vapor and subsequent condensation on the weld pool surface, the effect of the supply voltage, diameter and electrode feed rate on the distribution power and pressure of the arc on the surface of the arc cavity under a layer of flux;
- It is shown that the observed difference in the results of gas-shielded welding and submerged arc welding is associated with the redistribution of the heat generation power in the arc column by the processes of evaporation and condensation of the flux in the arc cavity;
- It is shown that the effect of arc voltage on the cross-sectional shape of the seam is related to the change in power redistributed by flux evaporation inside the arc cavity, as well as the location of the arc in the flux layer;
- It is shown that the diameter of the electrode on the cross-sectional shape of the seam is associated with changes in the power density and the flow pressure of electrode metal droplets onto the weld pool surface.

ACKNOWLEDGEMENTS

The work was carried out with the financial support of Ministry of Science and Higher Education of Russian Federation. The research results were obtained within the framework of the state task of the Ministry of Science and Higher Education of Russian Federation for the project № 9.12800.2018/12.2; applied science.
For the sponsorship and the support I wish to express my sincere gratitude.

REFERENCES

[1] T.Yamamoto, T. Ohji, F. Miyasaka , Y.Tsuji. Mathematical modeling of metal active gas arc welding. Science and Technology of welding and Joining. (2002). Vol. 7. No. 4. 260 – 264 pp.

[2] M.A. Sholokhov, V.A. Erofeev, S.I. Poloskov. A method for calculating the parameters of gas-shielded twin-arc multipass consumable electrode welding, Welding International. (2016). V. 30. № 7. pp. 541-547.

[3] Z.H. Rao, J. Hu, S.M. Liao, H.L. Tsai. GMAW using argon-helium mixtures. Part 1 -The arc. Int. J. Heat Mass Transfer. Modeling of the transport phenomena in 53(2010) 5707-5721.

[4] H.G. Fan, R. Kovacevic. A univied model of transport phenomena in gas metal arc welding including electrode, arc plasma and molten pool, J. Phys. D: Appl.Phys. 37(2004) 2531-2544 PII: S0022-37(04)77964-4

[5] Z.H. Rao, S.M. Liao, H.L. Tsai. Effects of shielding gas composition on arc plasma and metal arc welding. Journal of applied physic. 107, 044902, (2010).

[6] Zhang W., DebRoy T. Modelling of solidified free surface profile during GMA welding. Mathematical modelling and information technologies in welding and related processes. Proceedings of Seventh International Conference / Edited by Prof. I.V. Krivtsun, (Kiev: International Association «Welding»), 24 – 30 pp.

[7] P. Tekriwal, J. Mazumder, (1988) Finite element analysis of three-dimensional transient heat transfer in GMA welding. Weld J 67:150s–156s

[8] A. Mandal, R. Parmar, (2007) Numerical modeling of pulse MIG welding. ISIJ Int 47:1485–1490